

Piecewise Structural Diffusion Defined on Shape Index for Noise Reduction in Dual-Energy CT Images

Wenli Cai¹, June-Goo Lee^{1,2}, Da Zhang¹, Christina Piel^{1,3}, and Hiroyuki Yoshida¹

¹ 3D Imaging Research, Department of Radiology,
Massachusetts General Hospital and Harvard Medical School,
25 New Chardon St., Suite 400C, Boston, Massachusetts 02114, USA
{cai.wenli,yoshida.hiro}@mgh.harvard.edu

² Department of Radiology, University of Pittsburgh, 3362 Fifth Ave.
FARP/Imaging Research, Pittsburgh, Philadelphia 15213, USA

³ DInstitut für Medizinische Physik und Strahlenschutz, University of
Applied Sciences in Giessen, Wiesenstraße 14, 35390 Giessen, Germany

Abstract. The increasing radiation dose in dual-energy CT (DE-CT) scanning due to the double exposures at 80 kVp and 140 kVp is a major concern in the application of DE-CT. This paper presents a novel image-space denoising method, called *piecewise structural diffusion* (PSD), for the reduction of noise in low-dose DE-CT images. Three principle structures (plate, ridge, and cap) and their corresponding diffusion tensors are formulated based on the eigenvalues of a Hessian matrix. The local diffusion tensor that is piecewise-defined on the domain of shape index is composed by a linear combination of two diffusion tensors of the associated principle structures. A single diffusion tensor calculated from the fused DE-CT image is applied to both high- and low-energy images. In the DE-CT colon phantom study, we demonstrated that DE-CT images filtered by PSD yielded the similar image quality with half of radiation doses.

Keywords: Noise reduction, dual-energy CT, dual-energy CT colonography.

1 Introduction

The *dual-energy CT* (DE-CT) theory was first introduced by Alvarez and Macovski more than three decades ago [1]. With the recent technical advances, DE-CT became widely available in clinical practice. It provides an effective means for estimation of material composition by an analysis of two X-ray attenuation values acquired simultaneously at two photon energies (such as 80 kVp and 140 kVp). This ability of material decomposition has generated various new clinical applications that are otherwise unavailable in conventional single-energy CT [2].

Although DE-CT is highly promising, the potential of increased radiation dose, in the vicinity of one and half to two times of the dose of a routine single-energy CT examination due to the double exposures at 80 kVp and 140 kVp, is a major concern in the clinical application of DE-CT, because the potential risk of radiation-induced cancer due to the increasing radiation dose may not be negligible. Therefore, it is

imperative to lower the radiation dose of DE-CT to the level that is comparable to conventional single-energy CT without sacrificing the image quality.

Reduction of radiation dose (such as by lowering the tube current) may cause high image noise, low image contrast, and increased artifacts [3]. Major CT manufactures have been developing solutions to reducing radiation dose for DE-CT scanning, such as the automatic dose exposure control [4] and iterative reconstruction methods [5]. These methods are based on either the scanner hardware or the projection data (sinogram). An alternative solution is to apply noise reduction filters to reconstructed DE-CT images acquired with a low radiation dose, i.e., image-space denoising filters.

The purpose of this study is to develop a novel image-space DE-CT noise reduction filter called *piecewise structural diffusion* (PSD), and to evaluate the performance and the potential to reducing radiation dose, by using nine DE-CT datasets of a colon phantom scanned at various radiation doses.

The main contributions of the study are (1) PSD can deal with multiple structures in one diffusion process, and (2) a diffusion function is piecewise-defined on shape index [6-9]. Conventional diffusion filters works on only one type of structures, such as either tube or surface. We defined multiple principle structures (plate, ridge, and cap) based on anatomic features of interest, and used the scalar value of shape index to characterize a local 3D topologic shape. A local structure and its diffusion function were piecewise-defined on shape index. Our secondary contribution is to apply a single diffusion tensor to both high- and low-energy images in DE-CT, which takes advantages of both images for estimating a reliable local structure. We developed and demonstrated PSD filter in DE-CT colonography images.

2 Methods

2.1 Previous Work

Noise reduction filters have been developed and assessed for lowering image noise and improving image quality on CT images for decades [10]. Perona and Malik introduced the anisotropic diffusion process [11], in which smoothing is formulated mathematically as a diffusive process,

$$\frac{\partial}{\partial x} u(x, t) = \text{div}(D(x, t)\nabla u(x, t)), \quad (1)$$

where div is the divergence operator, ∇u is the gradient of the image and the diffusion strength is controlled by the diffusion tensor $D(x, t)$. $u(x, t)$ is the image intensity at spatial coordinate x and iteration step t .

In general, the diffuse tensor $D: R^{3 \times 3} \rightarrow R^{3 \times 3}$ is a matrix that enforces the directional preference of the diffusion along the principal directions. The diffusion tensor must satisfy C^∞ continuous, symmetric, and positive definite. Therefore, D is a symmetric positive definite matrix for a nonlinear anisotropic diffusion.

Conventional diffusion filters deals with one type of structures, such as edge-enhancing diffusion that enhances surface (edge) and coherent-enhancing diffusion

that enhances tube (line) [12]. However, anatomic structures may have different shapes in addition to surface and tube. In the context of CT colonography (CTC), colon contains surface shape for colonic walls, ridge shape for colonic folds, and cap shape for colonic polyps. Therefore, it is essential that a diffusion process can deal with multiple shapes in order to preserve different anatomic structures interested in images.

2.2 Principle Structure

Let $u(x)$ denote the CT value at a point $x \in R^3$ in a CT volume. The local morphological structure of $u(x)$ can be represented by a Hessian matrix $\nabla_{\sigma}^2 u(x)$, which is calculated by convolving $u(x)$ with the second Gaussian derivatives of a standard deviation σ . Let $|\lambda_1(x)| \leq |\lambda_2(x)| \leq |\lambda_3(x)|$ be the eigenvalues of $\nabla_{\sigma}^2 u(x)$ with corresponding eigenvectors of $e_1(x), e_2(x), e_3(x)$. A local morphologic structure can be characterized with a combination of the eigenvalues, called *eigenvalue signatures* [13].

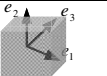
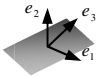
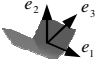

In general, a 3D diffuse tensor D can be defined as,

$$D(\nabla_{\sigma}^2 u(x)) = V(x)\Lambda(x)V(x)^T, \tag{2}$$

where $V(x) = [e_1(x), e_2(x), e_3(x)]$, $\Lambda(x) = \text{diag}[\tilde{\lambda}_1, \tilde{\lambda}_2, \tilde{\lambda}_3]$, and $\tilde{\lambda}_i$ ($0 < \tilde{\lambda}_i \leq 1$) is a positive-definite function of λ_i .

Table 1 illustrates the eigenvalue signatures and diffusion functions of different types of structures. Morphologically, if all eigenvalues are close to zero, there is no structure, i.e., it is a homogeneous region. A plate-like structure (such as colonic walls) has eigenvalue signature of $\lambda_1, \lambda_2 \approx 0; \lambda_3 \gg 0$. A ridge-like structure (such as colonic folds) has eigenvalue signature of $\lambda_1 \approx 0; \lambda_2, \lambda_3 \gg 0$. A cap-like structure (such as colonic polyps) has eigenvalue signature of $\lambda_1, \lambda_2, \lambda_3 \gg 0$. The sign of λ_i corresponds to convex/bright shapes ($\lambda_i \leq 0$) or concave/dark shape ($\lambda_i \geq 0$).

Table 1. Eigenvalue signatures and diffusion functions of principle structures

Morphological Category	Eigenvalue Signature	Diffusion Function
No structure (homogeneous) 	$\lambda_1, \lambda_2, \lambda_3 \approx 0$	(1,1,1)
Plate (colonic wall) 	$\lambda_1, \lambda_2 \approx 0;$ $\lambda_3 \gg 0$	$(1,1, \tilde{\lambda}_3^{plate})$
Ridge (colonic fold) 	$\lambda_1 \approx 0;$ $\lambda_2, \lambda_3 \gg 0$	$(1, \tilde{\lambda}_2^{Ridge}, \tilde{\lambda}_3^{Ridge})$
Cap (colonic polyp) 	$\lambda_1, \lambda_2, \lambda_3 \gg 0$	$(\tilde{\lambda}_1^{Cap}, \tilde{\lambda}_2^{Cap}, \tilde{\lambda}_3^{Cap})$

Because diffusion tensor D in equation (2) is required to be positive definite, all eigenvalues of D are positives. This also indicates that the diagonal element of $\Lambda(x)$ is positive definite, i.e., $\tilde{\lambda}_i^{ST} > 0$. Therefore, we assume, without loss of generality, that $\tilde{\lambda}_i^{ST}$ is a function of $|\lambda_i|$.

2.3 Diffusion Functions of Principle Structures

A diffusion function $\tilde{\lambda}_i^{ST}$ of a principle structure is defined as a function of eigenvalues. We define $\tilde{\lambda}_3^{ST}$ as a function of λ_3 :

$$\tilde{\lambda}_3^{ST}(\lambda_3) = \begin{cases} 1 & ; |\lambda_3| \leq H \\ 1 - \exp\left(\frac{-C}{(|\lambda_3| - H)^2}\right) & ; \text{otherwise,} \end{cases} \quad (3)$$

where H is a constant of eigenvalue to indicate whether there is a structure at point x (in the case of $|\lambda_3(x)| > H$), and $C = 2.0$ is a threshold parameter.

The diffusion functions $\tilde{\lambda}_1^{ST}$ and $\tilde{\lambda}_2^{ST}$ for a principle structure are calculated based on the ratios of $\frac{\lambda_1}{\lambda_3}$ and $\frac{\lambda_2}{\lambda_3}$:

$$\tilde{\lambda}_i^{ST}(\lambda_i) = \tilde{\lambda}_3^{ST} + (1 - \tilde{\lambda}_3^{ST}) \cdot \exp\left(-k \cdot \left(\frac{\lambda_i}{\lambda_3}\right)^2\right), \quad (4)$$

where $i = 1, 2$, and $k = 10$ is a threshold parameter.

In order to stop the diffusion at edges near zero-crossing, a weight function h is defined by use of the directional second derivative u_{nn} along the normal \mathbf{n} :

$$h(u_{nn}) = 1 - 0.9 \left(\frac{u_{nn}}{U}\right)^2, \quad (5)$$

where $U = 5$ is a threshold parameter. Note that $h = 0.0$ at zero-crossings.

The final diffusion function is formulated by $h(u_{nn}) * \tilde{\lambda}_i^{ST}(\lambda_i)$.

2.4 Shape Index

A shape index $SI(x)$ characterizes the local 3D topologic shape at a point $x \in R^3$ by use of the two principal curvatures κ_{max} and κ_{min} [6],[11],[12],[13]. Because the sign of a curvature defines the bending direction, i.e., inner or outer, a positive SI represents a convex shape, whereas a negative SI represents a concave shape. Under the condition of $\lambda_i \geq 0$, the shape index is defined by absolute value of curvatures as follows:

$$SI(x) = \frac{2}{\pi} \arctan\left(\frac{|\kappa_{max}| + |\kappa_{min}|}{|\kappa_{max}| - |\kappa_{min}| + \delta}\right), \quad (6)$$

where $\delta = 0.001$.

Fig. 1 illustrates that, by using equation (6), it is possible to determine to which of the three topologic shapes, plate, ridge, or cap, a point belongs based on a single value

of SI . The shape index is normalized between 0 and 1. Thus, point x that belongs to the plate shape has SI values around 0; ridge, around 0.5; and cap, around 1.0. The transition from one topologic shape to another occurs continuously.

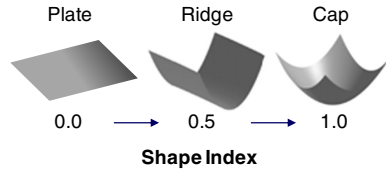


Fig. 1. Illustration of the relationship between the values of the shape index (equation (6)) and the corresponding shapes

2.5 Piecewise Structural Diffusion

Under the condition of $|\lambda_1| + |\lambda_2| + |\lambda_3| > 0$, the local shape at a point x can be represented as a combination of two principle structures, called *piecewise-defined structure*. Point x that has a combination of plate and ridge has $SI(x) < 0.5$; otherwise, it has a combination of ridge and cap. Therefore, a diffusion function is a piecewise function defined on $SI(x)$, called *piecewise structural diffusion* (PSD), as shown in equation (7).

$$\tilde{\lambda}_i = \begin{cases} (1 - w) \cdot \tilde{\lambda}_i^{Plate} + w \cdot \tilde{\lambda}_i^{Ridge}; & (0.0 \leq SI < 0.5) \\ (1 - w) \cdot \tilde{\lambda}_i^{Ridge} + w \cdot \tilde{\lambda}_i^{Cap}; & (0.5 \leq SI < 1.0), \end{cases} \quad (7)$$

where w is the weighting factor, which is in the range of $[0.0, 1.0]$.

Suppose that $P1$ and $P2$ are two principle structures at point x so that $SI^{P2} > SI^{P1}$. A simple form of w is a linear function of SI , as shown in equation (8).

$$w(x) = \frac{SI(x) - SI^{P1}}{SI^{P2} - SI^{P1}}. \quad (8)$$

2.6 Dual-Energy CT Diffusion

In DE-CT scanning, there are two CT values at a point x , $u_L(x)$ and $u_H(x)$, which are the CT values at low (80 kVp) and high (140 kVp) energies, respectively. In general, 80 kVp images provide greater contrast than that of 140 kVp, but its image quality is limited due to the increased noise. Because u_L and u_H are CT values at different photon energies of the same anatomic structures, the underlying diffusion structures are essentially the same for both images. Therefore, we applied a single diffusion tensor to both images as illustrated in Fig. 2.

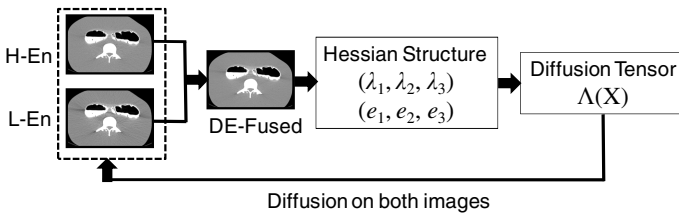


Fig. 2. Illustration of dual-energy CT diffusion iteration

The single diffusion tensor, $\Lambda(x)$, for both u_L and u_H was calculated by use of the fused images. Conventionally, high-energy and low-energy images are fused by a linear blending function: a mixing of 30% 80 kVp and 70% 140 kVp ($0.3 \cdot u_L(x) + 0.7 \cdot u_H(x)$).

3 Experiments and Results

We used a custom-ordered anthropomorphic colon phantom (Phantom Laboratory, Salem, NY) that was made of a urethane-mix material with a CT value of -100 ± 10 HU (120 kVp), and cast around simulated bony structures of a pelvis, 2 femurs, and 3 lumbar vertebrae. We installed a question-mark-shaped simulated colon with a length of approximately 50 cm and diameters of 3.5 ~ 4.0 cm. To simulate the semi-solid fecal materials in fecal-tagging CTC, we filled the colon phantom, prior to imaging, with 300 ml of simulated non-cathartic tagged fecal residues that were a mixture of aqueous fiber (psyllium), ground foodstuff (cereal), and non-ionic iodinated contrast agent (Omnipaque iohexol, GE Healthcare) at a concentration of 40 mg/ml.

The phantom was scanned on a DE-CT scanner (SOMATON Definition Flash, Siemens Healthcare) with two different photon voltages: 80 kVp and 140 kVp. We applied nine tube current settings, 12 ~ 74 mAs for 140 kVp and 60 ~ 370 mAs for 80 kVp, to test image noise at different radiation doses. The radiation dose index (CTDIvol) ranged from 2.79 to 16.77 mGy. For all scanning, we applied the soft tissue reconstruction algorithm and a 0.625 mm slice reconstruction interval. In total, we generated nine DE-CT datasets (512x512x537) for testing.

We used the same parameter settings for all of our denoising experiments. With a unit grid spacing in all dimensions, we empirically set $\Delta t = 0.125$ for a stable numeric iteration of the diffusion equation (1). The number of iterations in the diffusion process was set to 50. The standard deviation of Gaussian derivatives for calculation of Hessian matrix and eigenvalues was set to $\sigma = 1.0$.

For the assessment of the image quality after noise reduction, two groups of image quality metrics were evaluated:

- To measure the noise level of the images: the mean (μ) and standard deviation (SD) of the images.
- To measure the local structure similarity: quality index of local variance (QILV) [11] (value range [0.0, 1.0]) referred to the images scanned at the highest radiation dose.

Table 2 lists the measurements of mean SD (MSD) and QILV for both original and denoised images at 140 kVp and 80 kVp. By comparison of the shaded cells in the table, we observed that the PSD filter can reduce the radiation dose approximately 50% for the 140 kVp images and more than 50% for the 80 kVp images.

Fig. 3 demonstrates an example of the effect of PSD on the reduction of radiation dose. The images at the upper row are the original images scanned at a CTDIvol of 13.65 mGy, and the lower row shows the PSD-denoised images that were scanned at a CTDIvol of half of the dose, i.e., 6.83 mGy. Both groups of images have the same

Table 2. Comparison of mean standard deviation (MSD) and quality index of local variance (QILV) in both 140 kVp and 80 kVp images

Dose (mGy)	140 kVp Images				80 kVp Images			
	Original		Denoised		Original		Denoised	
	MSD	QILV	MSD	QILV	MSD	QILV	MSD	QILV
2.79	69.2	0.86	49.0	0.97	97.1	0.93	63.0	0.97
3.50	66.5	0.90	45.9	0.98	85.1	0.95	52.8	0.98
4.65	55.9	0.94	36.2	0.99	79.0	0.97	48.4	0.98
6.83	46.9	0.98	26.6	0.99	69.2	0.98	39.0	0.99
9.10	41.0	0.99	21.0	0.99	67.4	0.99	36.2	0.99
11.34	38.0	0.99	19.5	0.98	61.4	0.99	32.1	0.98
13.65	35.6	0.99	17.8	0.98	51.2	0.99	25.9	0.98
15.92	30.8	0.99	14.3	0.98	48.4	0.99	26.3	0.98
16.77	30.4	1.00	13.6	0.99	48.0	1.00	25.7	0.99

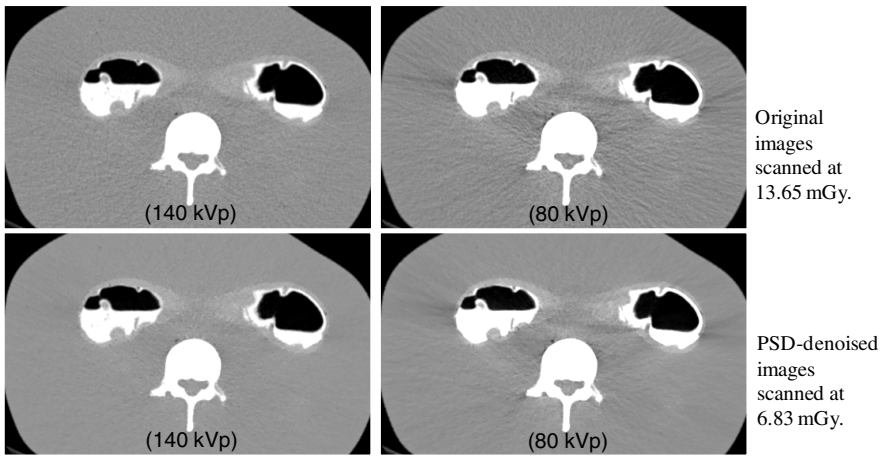


Fig. 3. An example of the effect of PSD filter on the reduction of radiation dose. The upper row shows the original images scanned at 13.65 mGy with MSD of 35.6 (140 kVp) and 51.2 (80 kVp). The lower row shows the denoised images scanned at 6.83 mGy with MSD of 26.6 (140 kVp) and 39.0 (80 kVp). Both groups have the same QILV of 0.99.

QILV values, i.e., the same level of structure similarity referred to the images scanned at the highest dose. However, the MSD of the images scanned at 13.65 mGy (upper row) were 35.6 (140 kVp) and 51.2 (80 kVp), whereas the MSD of the PSD-denoised images scanned at 6.83 mGy (lower row) were 26.6 (140 kVp) and 39.0 (80 kVp), respectively. We observed that the half-dose DE-CT images have less noise after the application of PSD filter than that of the full-dose images.

We compared the performance of PSD with six other denoising methods: binomial filter (BF), Gaussian filter (GF), curvature anisotropic diffusion (CAD), curvature flow (CF), gradient anisotropic diffusion (GAD), and min/max curvature diffusion (MMCD) by use of the recommended parameters [14]. We compared the SDs before

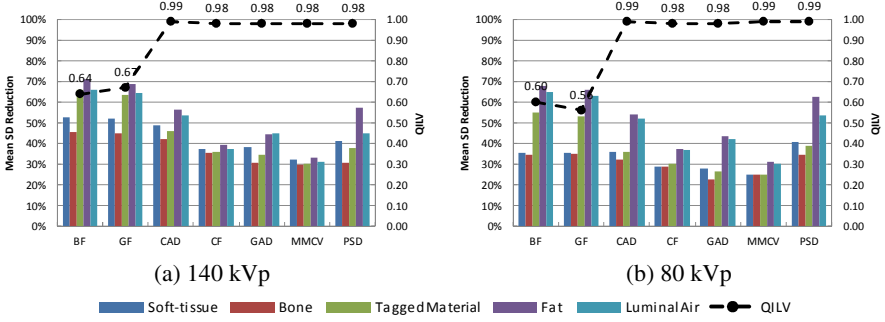


Fig. 4. Comparisons of seven denoising algorithms: binomial filter (BF), Gaussian filter (GF), curvature anisotropic diffusion (CAD), curvature flow (CF), gradient anisotropic diffusion (GAD), min/max curvature diffusion (MMCD), and the proposed PSD, in (a) 140 kVp images and (b) 80 kVp images. The left vertical axis is the mean SD reduction: $R_{SD} = (SD_{source} - SD_{filtered})/SD_{source} \cdot 100\%$, which measures the performance on noise reduction. The color bars show the mean R_{SD} in five materials. The right vertical axis is the mean QILV. The dashed line displays the mean values of QILV of the filtered images referred to the highest dose images.

and after application of seven denoising algorithms on five materials: soft-tissue, bone, tagged materials, fat, and luminal air. The noise reduction rate is define as $R_{SD} = (SD_{source} - SD_{filtered})/SD_{source} \cdot 100\%$. Mean R_{SD} values of nine datasets are compared by the color bars in Fig. 4 for both 140 kVp and 80 kVp images. In addition, we measured the QILV referred to the highest dose images to compare the effect of preservation of structural details after denoising. We observed that, although BF and GF had a high noise reduction rate, their QILV values were low compared to the other five diffusion filters. These results show that both BF and GF removed image noise by losing image details, which tend to blur the images. On the other hand, five diffusion filters showed better performance on detail preservation as indicated by the high QILV values. Among five diffusion filters, PSD performed better on noise reduction than other diffusion filters, especially in the low-energy images.

4 Conclusions

Image-space noise reduction filter is an alternate means for lowering the radiation dose in DE-CT. This paper presents a novel anisotropic diffusion filter called PSD that used a piecewise structural diffuse tensor for preserving multiple types of structures in DE-CT images. The proposed PSD filter was evaluated by use of nine DE-CT datasets of a colon phantom scanned at various radiation doses. The results demonstrated that the application of PSD may reduce more than half of the radiation dose in DE-CT scanning. In addition, PSD outperformed other diffusion filters on noise reduction in DE-CT images, especially in low-energy images. Further clinical studies will be conducted to demonstrate the performance of PSD filter on low-dose DE-CTC-based colon cancer screening and other clinical applications such as the electronic cleansing [15-17].

Acknowledgements. The project described was partly supported by Research Scholar Grant RSG-11-076-01-CCE from the American Cancer Society, and by Grant Numbers R01CA095279, R01CA131718, and R03CA156664 from National Cancer Institute (NCI).

References

1. Alvarez, R.E., Macovski, A.: Energy-Selective Reconstructions in X-Ray Computerised Tomography. *Phys. Med. Biol.* 21, 733–744 (1976)
2. Johnson, T., Fink, C., Schönberg, S.O., Reiser, M.F.: *Dual Energy CT in Clinical Practice* (2011)
3. Kalra, M.K., Maher, M.M., Toth, T.L., Hamberg, L.M., Blake, M.A., Shepard, J.A., Saini, S.: Strategies for CT Radiation Dose Optimization. *Radiology* 230, 619–628 (2004)
4. Murazaki, H., Funama, Y., Sugaya, Y., Miyazaki, O., Tomiguchi, S., Awai, K.: Optimal Setting of Automatic Exposure Control Based on Image Noise and Contrast on Iodine-Enhanced CT. *Acad. Radiol.* (2012)
5. Silva, A.C., Lawder, H.J., Hara, A., Kujak, J., Pavlicek, W.: Innovations in CT Dose Reduction Strategy: Application of the Adaptive Statistical Iterative Reconstruction Algorithm. *AJR Am. J. Roentgenol.* 194, 191–199 (2010)
6. Koenderink, J.J.: *Solid shape*. MIT Press, Cambridge (1990)
7. Yoshida, H., Näppi, J.: Three-Dimensional Computer-Aided Diagnosis Scheme for Detection of Colonic Polyps. *IEEE Trans. Med. Imaging* 20, 1261–1274 (2001)
8. Yoshida, H., Näppi, J., MacEneaney, P., Rubin, D.T., Dachman, A.H.: Computer-Aided Diagnosis Scheme for Detection of Polyps at CT Colonography. *Radiographics* 22, 963–979 (2002)
9. Yoshida, H., Masutani, Y., MacEneaney, P., Rubin, D.T., Dachman, A.H.: Computerized Detection of Colonic Polyps at CT Colonography on the Basis of Volumetric Features: Pilot Study. *Radiology* 222, 327–336 (2002)
10. Alvarez, R.E., Stonestrom, J.P.: Optimal Processing of Computed Tomography Images using Experimentally Measured Noise Properties. *J. Comput. Assist. Tomogr.* 3, 77–84 (1979)
11. Perona, P., Malik, J.: Scale-Space and Edge Detection using Anisotropic Diffusion. *IEEE Trans. Pattern Anal. Mach. Intell.* 12, 629–639 (1990)
12. Weickert, J., Heidelberglaan, E.: *A Review of Nonlinear Diffusion Filtering* (1997)
13. Sato, Y., Westin, C., Bhalerao, A., Nakajima, S., Shiraga, N., Tamura, S., Kikinis, R.: Tissue Classification Based on 3D Local Intensity Structures for Volume Rendering. *IEEE Trans. Visualization and Computer Graphics* 6, 160–180 (2000)
14. Ibanez, L., Schroeder, W., Ng, L., Cates, J.: *The ITK Software Guide*, 2nd edn. Kitware Inc. (2005)
15. Cai, W., Lee, J.G., Zalis, M.E., Yoshida, H.: Mosaic Decomposition: An Electronic Cleansing Method for Inhomogeneously Tagged Regions in Noncathartic CT Colonography. *IEEE Trans. Med. Imaging* 30, 559–574 (2011)
16. Cai, W., Yoshida, H., Zalis, M.E., Näppi, J.J., Harris, G.J.: Informatics in Radiology: Electronic Cleansing for Noncathartic CT Colonography: A Structure-Analysis Scheme. *Radiographics* 30, 585–602 (2010)
17. Cai, W., Zalis, M.E., Näppi, J., Harris, G.J., Yoshida, H.: Structure-Analysis Method for Electronic Cleansing in Cathartic and Noncathartic CT Colonography. *Med. Phys.* 35, 3259–3277 (2008)